2D Materials

PAPER

Barkhausen effect in the first order structural phase transition in type-II Weyl semimetal $MoTe_2$

2D Materials

PAPER

Barkhausen effect in the first order structural phase transition in type-II Weyl semimetal $MoTe_2$

RECEIVED
30 June 2018

REVISED
18 August 2018

ACCEPTED FOR PUBLICATION
12 September 2018

PUBLISHED
17 October 2018

Chuanwu Cao[1,2], Xin Liu[1,2], Xiao Ren[1,2], Xianzhe Zeng[1,2], Kenan Zhang[2,3], Dong Sun[1,2], Shuyun Zhou[2,3], Yang Wu[4], Yuan Li[1,2] and Jian-Hao Chen[1,2]

[1] International Center for Quantum Materials, School of Physics, Peking University, NO. 5 Yiheyuan Road, Beijing, 100871, People's Republic of China
[2] Collaborative Innovation Center of Quantum Matter, Beijing 100871, People's Republic of China
[3] State Key Laboratory of Low Dimensional Quantum Physics, Department of Physics, Tsinghua University, Beijing 100084, People's Republic of China
[4] Tsinghua-Foxconn Nanotechnology Research Center, Tsinghua University, Beijing 100084, People's Republic of China

E-mail: chenjianhao@pku.edu.cn

Keywords: 2D materials, Barkhausen effect, structural phase transition, $MoTe_2$

Supplementary material for this article is available online

Abstract

We report the first observation of the non-magnetic Barkhausen effect in van der Waals layered crystals, specifically, during transitions between the T_d and $1T'$ phases in type-II Weyl semimetal $MoTe_2$. Thinning down the $MoTe_2$ crystal from bulk material to about 25 nm results in a drastic strengthening of the hysteresis in the phase transition, with the difference in critical temperature increasing from ~40 K to more than 300 K. The Barkhausen effect appears for thin samples and the temperature range of the Barkhausen zone grows approximately linearly with reducing sample thickness, pointing to a surface origin of the phase pinning effects. The distribution of the Barkhausen jumps shows a power law behavior, with its critical exponent $\alpha = 1.27$, in good agreement with existing scaling theory. Temperature-dependent Raman spectroscopy on $MoTe_2$ crystals of various thicknesses shows results consistent with our transport measurements.

Introduction

Layered transition metal dichalcogenides (TMDs), a family of van der Waals crystals, have attracted extensive research interests due to their intriguing properties [1–4]. Certain TMDs have rich structural and electronic phases which exhibit drastically different physical properties [5–15]. $MoTe_2$, in particular, is an excellent example of such multi-phase materials, which possesses three different crystal structures: hexagonal $2H$, monoclinic $1T'$, and orthorhombic T_d [14]. The $2H$ phase $MoTe_2$ is a semiconductor and candidate material for 2D field effect transistors (2D-FETs) [16]. The $1T'$ phase $MoTe_2$ is a quantum spin Hall candidate at the single layer form [17, 18], and a central symmetric semimetal at the multi-layer form, whose crystal symmetry belongs to the $P2_1/m$ space group [14]. The non-centrosymmetric T_d phase $MoTe_2$ belongs to the $Pmn2_1$ space group and is a type-II Weyl semimetal which violates the Lorentz invariant, with the Weyl points appear as the touching points between electron and hole pocket in a tilted cone configuration [14,15].

The structural phase transition of $MoTe_2$ between the $1T'$ phase and the $2H$ phase can be achieved by electrostatic doping at room temperature [8], while the transition between the $1T'$ phase and the T_d phase is driven by temperature [14]. Such temperature driven structural phase transition between T_d (low temperature phase) and $1T'$ (high temperature phase) has been demonstrated by electrical transport [19, 20], Raman spectroscopy [14] and angle-resolved photoemission spectroscopy [15]. In this article, we report the first observation of Barkhausen physics in the first order structural phase transition between the two metallic phases of $MoTe_2$ (the $1T'$ phase and the T_d phase).

The Barkhausen effect is originally defined as a series of sudden reversal of Weiss domains in a ferromagnet during a continuous process of magnetization or demagnetization [21–23]. The Barkhausen physics is related to domain wall pinning and de-pinning when a ferromagnetic system experiences a transition between two different states. During the transition, the domain wall between two states moves through the sample. Defects in the crystal pin the moving domain

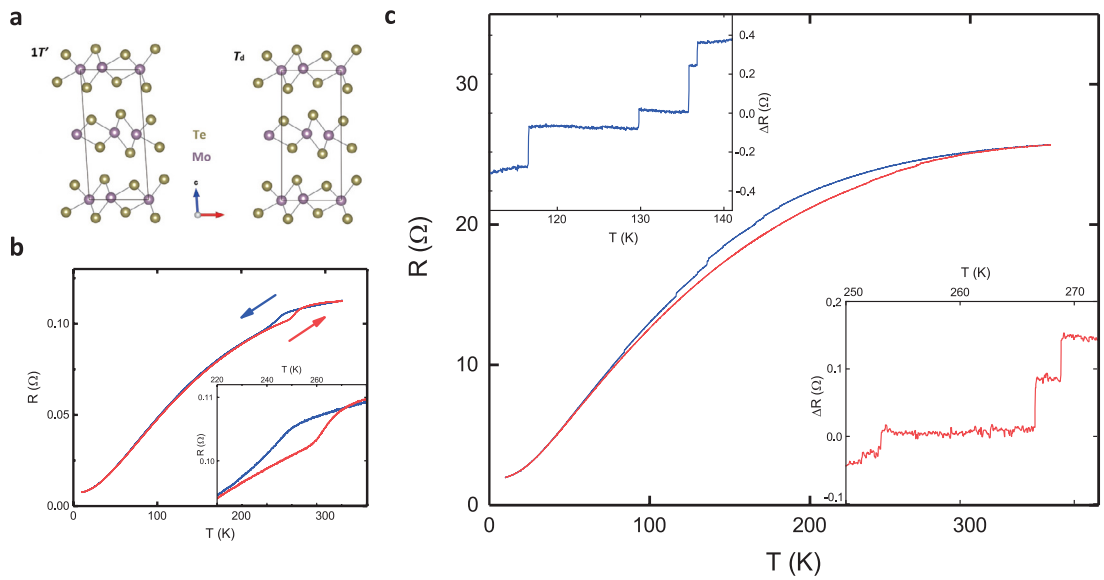

Figure 1. Temperature-induced phase transition in few-layer $MoTe_2$. (a) Crystal structures of $1T'$ and T_d phase $MoTe_2$. (b) Temperature dependent resistivity of a bulk $MoTe_2$ sample; cooling curve in blue, warming in red. (c) Temperature dependent resistivity of a 50 nm $MoTe_2$ sample. Cooling curve in blue, warming in red. Upper (lower) insets: zoom-in of the cooling (warming) curve in (c) with background subtracted.

wall and hold the neighbor area in the past state until the energy gain in flipping the whole neighbor area gets larger than the de-pinning energy. When de-pinning happens, the pinned area suddenly turns into the other state, leading to a jump in the total magnetization of the sample (see supplementary materials figure S1 (stacks.iop.org/TDM/5/044003/mmedia)). The Barkhausen effect has been a powerful tool to characterize magnetic and ferroelectric materials [24–27], and it has also attracted growing interest as an example of complex dynamical systems displaying dimension-dependent scaling behavior [22]. Given the ubiquitous presence of the Barkhausen effect in magnetic phase transition [24–29], only a limited number of research has revealed Barkhausen physics in thermally-driven first-order phase transition in non-magnetic materials [30–35], and none of such transition has been observed in van der Waals layered crystals.

Here, we report the first observation of the thickness-dependent Barkhausen effect in the thermally-driven first order structural phase transition between the T_d phase and the $1T'$ phase in $MoTe_2$. The T_d phase and $1T'$ phase $MoTe_2$ are both metallic but with different resistivity at any given temperature (e.g. $\rho_{T_d} < \rho_{1T'}$). Thus, careful measurement of the resistivity of the $MoTe_2$ as a function of temperature $\rho(T)$ reveals events of the structural phase transition in the crystal.

For bulk crystals, the phase transition happens sharply at around 250 K with no additional features, and hysteresis of the transition temperature, defined as $T_{\text{hysteresis}} = T_{T_d \to 1T'} - T_{1T' \to T_d}$, is around 40 K (figure 1(b)). For samples between 100 nm–20 nm, on the other hand, the phase transition occurs in a large temperature region and exhibits a series of kinks in $\rho(T)$, which is a manifestation of the Barkhausen effect. Thinning down the $MoTe_2$ crystal from bulk material to about 20 nm results in a drastic strengthening of the hysteresis in the phase transition, with $T_{\text{hysteresis}}$ increasing from ~40 K to more than 300 K. The temperature range of the Barkhausen zone grows approximately linearly with reducing sample thickness as determined by four-probe resistivity measurement. The distribution of the Barkhausen jumps shows a power law behavior, with its critical exponent $\alpha = 1.27$, consistent with theoretical expectations as explained later in this letter. Temperature-dependent Raman spectroscopy is also performed on $MoTe_2$ crystals of various thicknesses, showing results consistent with our transport measurements.

Results and discussion

The temperature-driven structural phase transition in few-layer metallic $MoTe_2$ is studied using electrical transport measurement as well as Raman spectroscopy. Figure 1(a) shows the atomic schematics of $MoTe_2$ in T_d phase and in $1T'$ phase. The T_d phase $MoTe_2$ shares the same in-plane crystal structure with the $1T'$ phase $MoTe_2$ and differs only in vertical stacking [14]. Figure 1(b) shows a typical temperature-dependent four-probe resistivity curve of bulk metallic $MoTe_2$. The transition from $1T'$ phase to T_d phase occurs at about 230 K to 250 K and the transition from T_d phase to $1T'$ phase occurs at about 260 K to 270 K. It is experimentally observed that $\rho_{T_d} < \rho_{1T'}$ at the phase transition temperature, thus $\Delta\rho_{T_d \to 1T'} > 0$ and $\Delta\rho_{1T' \to T_d} < 0$.

Figure 1(c) shows a typical temperature-dependent four-probe resistivity curve $\rho(T)$ for a 50 nm-thick $MoTe_2$ sample, which is fairly different from that of the bulk samples. The cooling curve and warm-

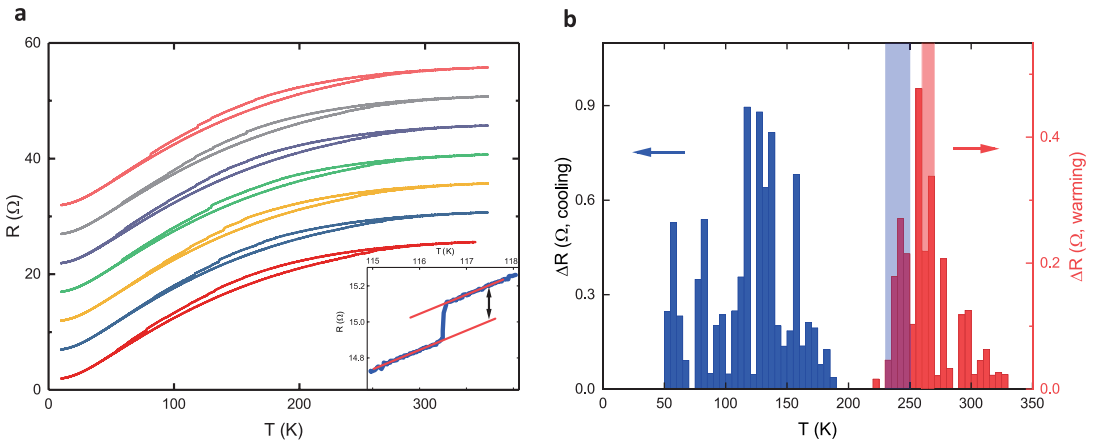

Figure 2. Barkhausen jumps in few-layer $MoTe_2$. (a) Repeated temperature dependent resistivity measurement of the 50 nm $MoTe_2$ sample. Seven runs of the cooling-warming process are plotted together with Y-offset. The inset shows the method to determine kink height. (b) Histogram of resistivity kinks in figure (a), weighted by kink's height. Kinks in cooling and warming are plotted side-by-side. Blue- and red-shaded area is the phase transition region for bulk $MoTe_2$ crystals during cooling and warming, respectively.

ing curve do not overlap from 80 K to 320 K, showing that the hysteresis of transition between the $1T'$ phase and the T_d phase has been strengthened. While bulk crystals show a smooth function of $\rho(T)$ during the phase transition, a series of kinks in $\rho(T)$ appear in a wide temperature range for both the warming and cooling curves in thinner samples. Here a kink means an instance of rapid change in the $\rho(T)$ curve. We found that all the kinks in the cooling curve ($1T' \rightarrow T_d$, upper inset in figure 1(c)) represent rapid drops in the resistivity, while all the kinks in the warming curve ($T_d \rightarrow 1T'$, lower inset in figure 1(c)) represent rapid increase in the resistivity, consistent with the fact that $\Delta\rho_{1T'\rightarrow T_d} < 0$ and $\Delta\rho_{T_d\rightarrow 1T'} > 0$. Thus, both the kinks and the strengthened hysteresis behavior in the $\rho(T)$ curves can be attributed to modified structural phase transition in thin $MoTe_2$ crystals. The appearance of kinks in the $\rho(T)$ curves reveals the existence of phase pinning in the first order phase transition process in thin $MoTe_2$. During cooling (warming) process, defects or local strains in the crystal pin their neighbor area in the $1T'$ (T_d) phase; as the temperature becomes sufficiently low (high), the pinned area suddenly flips to the T_d ($1T'$) phase, and be detected as a kink in the $\rho(T)$ curves.

Figure 2(a) shows $\rho(T)$ curves for seven temperature scans of a 50 nm $MoTe_2$ sample between 10 K and 350 K (curves offset for clarity). All the curves show metallic and hysteresis behavior. We found that kinks in the $\rho(T)$ curves do not happen at the same temperature during different experimental runs for the same device, but rather, has a statistical distribution, which is analogous to the Barkhausen effect observed in magnetic materials (e.g. jumps in the $M(H)$ curves has a statistical distribution) [24, 25]. The distribution of the kinks can be summarized as a histogram of the occurrence of the kinks weighted by the height ($\Delta\rho$) of respective kinks, as shown in figure 2(b). We collect kinks from all 7 runs of cooling and warming process, sum up all kinks' height in each bin (5 K in temperature), and plot the value (in units of Ohms) as a function of temperature. The height of a kink is obtained using a procedure shown in the inset of figure 2(a). It is worth pointing out that the kink histogram may not show the full scale of the phase transition, but rather, show the temperature distribution of all the detected Barkhausen jumps. Nonetheless, the kink histogram reveals the temperature range that phase transition occurs. In figure 2(b), the blue histogram is extracted form cooling curves, and red from warming curves. Comparing with the bulk, the temperature range of the phase transition shifts and expands to 180 K–50 K for the $1T' \rightarrow T_d$ transition, and 230 K–320 K for the $T_d \rightarrow 1T'$ transition. The expansion of $T_{hysteresis}$ can also be explained by the Barkhausen effect, as defects pinning impedes the phase transition process, leading to super-cooled/super-heated states. We notice that the total-height of the Barkhausen jumps in cooling is much larger than in warming. One possible explanation is that the pinning effect is stronger as thermal fluctuation is smaller in lower temperature, thus larger Barkhausen jumps are recorded during cooling than during warming.

To study the evolution of the phase transition temperature as a function of sample thickness, we fabricated several devices with thickness ranging from 6 nm to 120 nm. For samples between 20 nm–100 nm, the Barkhausen effect can be observed. We can define the 'Barkhausen zone' as the range of temperature between the highest and the lowest kink temperature. For samples thicker than 100 nm, Barkhausen jumps disappear and the $\rho(T)$ curves show bulk-like behavior with a shift of the transition temperature (see supplementary materials figure S2). Figure 3 plots the temperature ranges of the Barkhausen jumps versus sample thickness together with the phase transition temperature range for bulk crystals. The temperature ranges are plotted by dash bars for each thickness. We

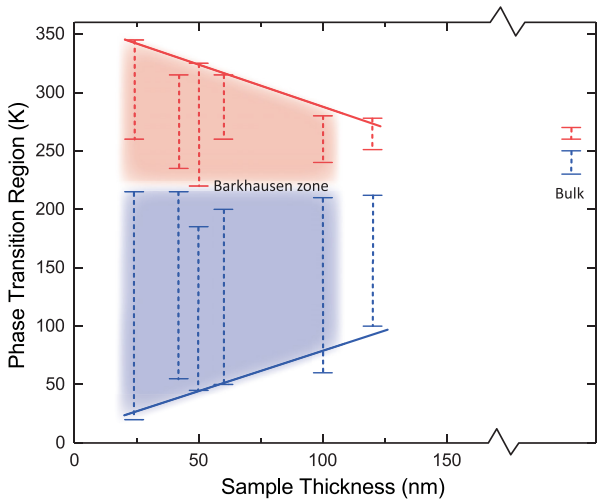

Figure 3. Thickness dependent phase transition temperature ranges. Barkhausen zone as a function of sample thickness. Barkhausen zone is extracted by the highest/lowest temperature that Barkhausen jumps appear, and are plotted by blue bars and red bars for cooling and warming, respectively. Shaded area denotes the parameter space of temperature and sample thickness where Barkhausen effect is detected. For sample thicker than 100 nm, the endpoints are determined by the temperature at which cooling and warming curves begins to overlap.

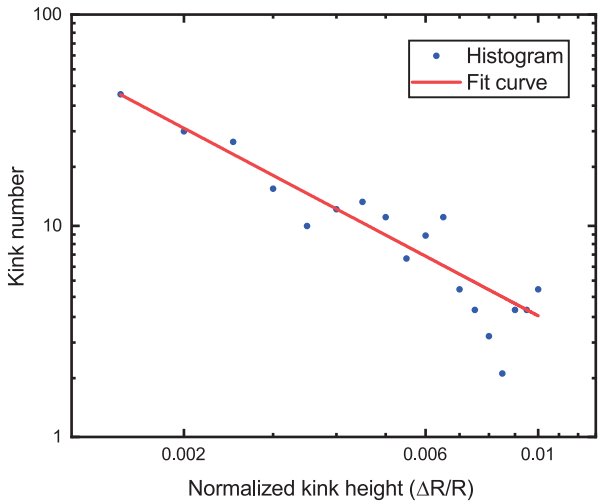

Figure 4. Distribution of normalized resistivity kink height. Histogram of normalized resistivity kink height $\Delta R/R$ for all the samples (blue dots), where R is the sample resistivity at the resistivity jump, and ΔR is the respective jumps in resistivity. Red line shows a power law fitting. Exponent $\alpha = 1.27 \pm 0.08$ is obtained from the fit.

find that both the upper bound and the lower bound of the Barkhausen zone extend approximately linearly when sample thickness is reduced. This phenomenon infers that the pinning effect enhances linearly when sample's layer number decreases, suggesting a possible surface origin of the pinning effects. In contrast to the Barkhausen effect observed in ferromagnets, where the phase pinning is generally believed to originate from lattice defects [22, 23], little is known about the exact nature of the 'phase pinning defects' in thin $MoTe_2$. The phase boundary of T_d and $1T'$ $MoTe_2$ is basically a stacking fault which could be pinned for various causes. First of all, one reasonable ansatz is that such surface related pinning comes from local strains at the $MoTe_2$/substrate interface, where the corrugated, amorphous SiO_2 substrate induced a random distribution of strain at the $MoTe_2$ sample. Thinner samples conform better to such substrate corrugation, thus results in higher strain. Secondly, the likely presence of residual photoresist at the surface of the thin $MoTe_2$ samples could also be a source of local strain which results in phase pinning. The third possibility is that atomic defects at the $MoTe_2$ samples [36] can act as phase pinning defects, but it is highly unclear why more defects appears in thinner samples, since mechanical exfoliation and e-beam lithography are gentle device fabrication techniques, which should not result in additional defects in the samples. The exact nature of such surface related pinning effects will be an interesting topic in future local probe experiments. No transition signal is observed for samples at or below 6 nm (see supplementary materials figure S4). Since

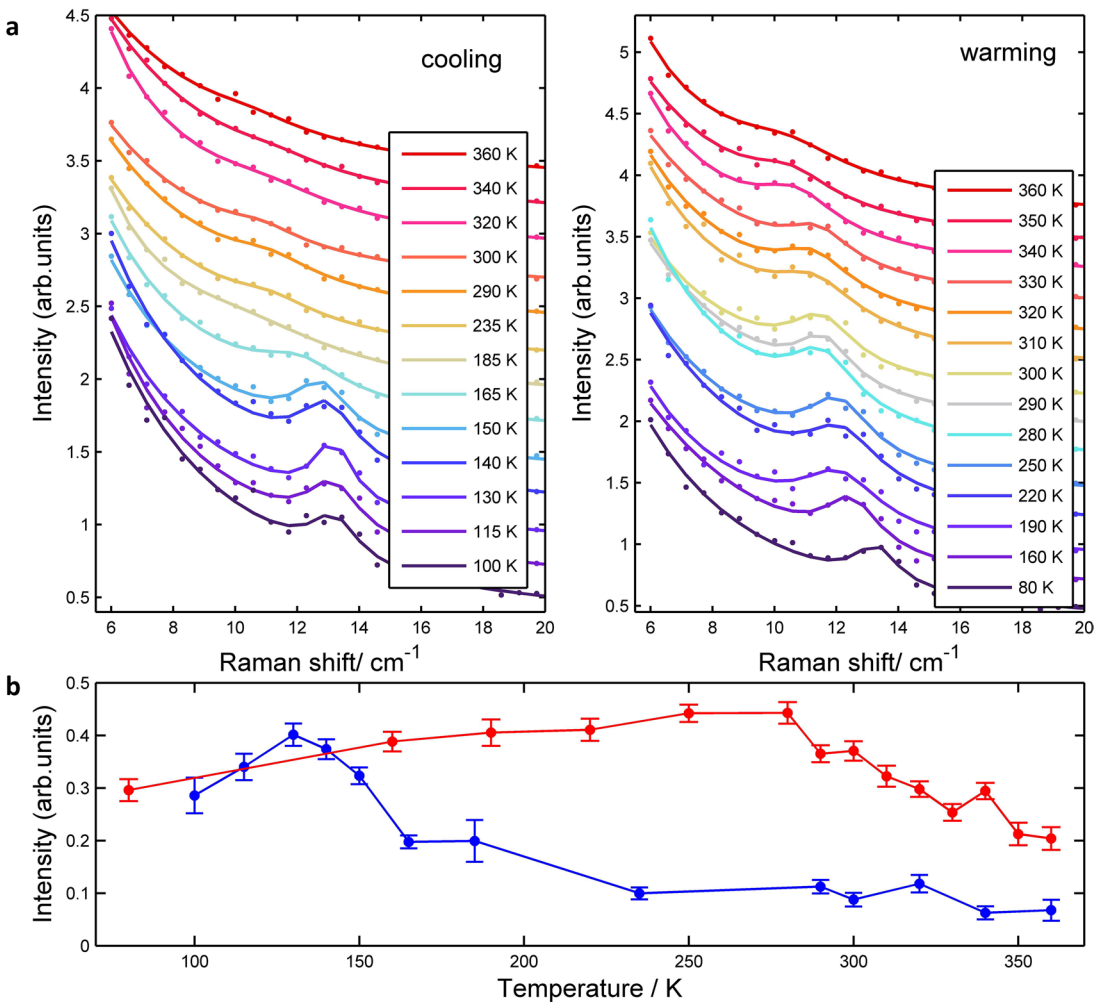

Figure 5. Temperature dependence of polarized Raman spectra for the signal at 13 cm^{-1}. Temperature dependent Raman spectra around 13 cm^{-1} for (a) a 22 nm sample, (c) a 155 nm sample. Temperature dependence of the Raman intensity for the 13 cm^{-1} peak for (b) a 22 nm sample, (d) a 155 nm sample. Blue for cooling and red for warming in (b) and (d).

$1T'$ and T_d $MoTe_2$ share the same in-plane structure [14], the phase transition behavior towards the monolayer limit warrants further investigation.

Figure 4 plots the histogram of the normalized resistivity kink height ($\Delta R/R$) for all the devices measured. Here $\Delta R = R_{1T'} - R_{T_d}$ represents ~5% of the total resistivity of the sample, thus we can assign the total resistivity of the sample $R = R_{1T'} \cong R_{T_d}$. We found that the distribution function f of $\Delta R/R$ from all the devices we measured follows a power law $f \sim (\Delta R/R)^{-\alpha}$, with $= 1.27 \pm 0.08$. Theoretically, it has been predicted that the domain size (s) of each Barkhausen jump has a distribution P that follows a power law $P(s) \sim s^{-\beta}$ [22, 23, 28]. Mean-field theory gives a universal exponent $\beta = 2 - 2/(d+1)$ for such power law behavior, where $d \leqslant 3$ is the dimension of the system [23]. It is reasonable to assume that ΔR is proportional to the total resistivity R for a given size of flipped domain at any given temperature, thus the size of the flipped domain $s \sim \Delta R/R$. If the Barkhausen effect in thin $MoTe_2$ is 3D, then $\beta = 1.5$, which does not agree with our experimental observation. On the other hand, if there are mainly 2D phase pinning/depinning in thin $MoTe_2$, then $\beta = 4/3 \approx 1.33$, which agrees well with the experimentally extracted value of α. This result suggests that the phase transition between $1T'$ and T_d in thin $MoTe_2$ could be a rare example for non-magnetic Barkhausen effect in the 2D universality class. It is worth noting that the theories describing scaling behavior in a Barkhausen process in magnetic materials is far from united, much less is known for Barkhausen process in non-magnetic structural phase transition. For example, an elastic interface theory predicts $\beta \approx 1.3$ for a 3D magnetic Barkhausen process [23, 37, 38]. Thus more theoretical study is needed to fully understand our experimental observation.

As a further verification of the shifting and expansion of the phase transition temperature, we performed temperature-dependent polarized Raman spectroscopy on thin $MoTe_2$ samples. The strongest Raman signal that distinguishes the $1T'$ and the T_d phases is the interlayer shear mode at ~13 cm^{-1}, as measured in the parallel-polarized configuration [14]. Centrosymmetry breaking in the T_d structure leads to a Raman active mode at 13 cm^{-1} (denoted as the A peak), whereas this mode is Raman inactive in $1T'$ $MoTe_2$. Figure 5(a) shows the Raman spectra between 6 cm^{-1} and 20 cm^{-1} of a 22 nm-thick $MoTe_2$ sample at different temper-

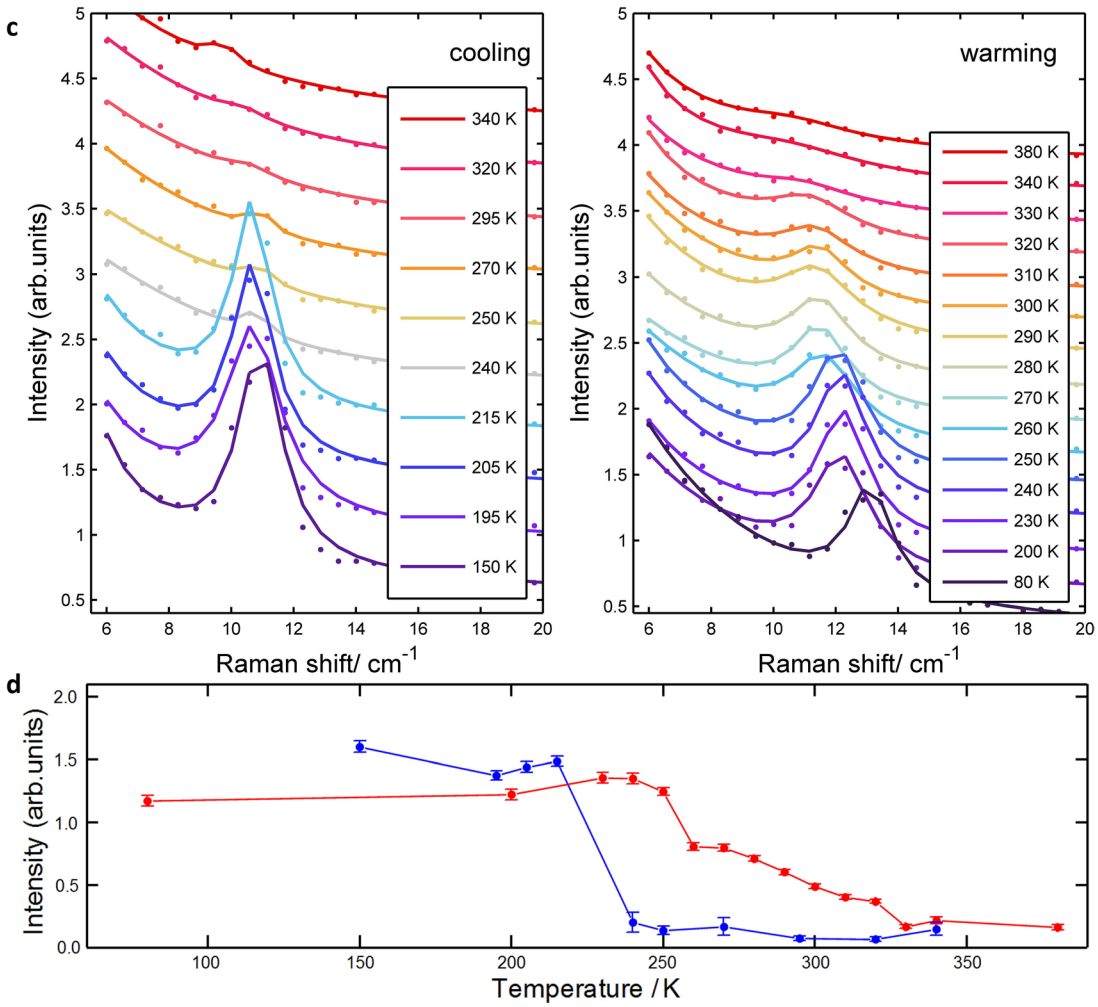

Figure 5. (*Continued*)

ature during sample cooling (left panel) and warming (right panel). The temperature-dependent evolution of the intensity of the A peak is shown in figure 5(b). One can find that the intensity of the peak increases between 235 K and 130 K during sample cooling, and starts to decrease above 280 K during sample warming. Up to 350 K, the A peak is still observable for the 22 nm sample. This is in stark contrast to bulk $MoTe_2$, where such change in the intensity of the A peak is completed within 215 K to 280 K [14]. Figure 5(c) is the temperature-dependent Raman spectra of a 155 nm-thick $MoTe_2$ sample between 6 cm^{-1} and 20 cm^{-1}, which shows intermediate behavior between bulk and the 22 nm-thick $MoTe_2$. The observation in figure 5 is consistent with resistivity measurement, showing enhancing $T_{hysteresis}$ with samples of reducing thickness.

Conclusions

We report the first observation of the Barkhausen effect in the first order structural phase transition between the two metallic phases, e.g. the 1T' phase and the T_d phase, of $MoTe_2$ thin flakes. The temperature range of the Barkhausen zone increase linearly with reducing thickness, pointing to a surface origin of the phase pinning defects. The distribution of normalized resistivity jumps ($\Delta R/R$) has a power law dependence with exponent $\alpha = 1.27 \pm 0.08$, suggesting an underlying scaling behavior. Temperature-dependent Raman spectroscopy also detects thickness dependent temperature ranges for the phase transition, consistent with data from transport measurement.

Methods

The bulk 1T' $MoTe_2$ crystals were synthesized by chemical vapor transport method [15, 39–43], and few-layer samples were mechanical exfoliated from bulk crystals and deposited onto silicon wafer with 300 nm SiO_2. Standard electron beam lithography and metallization processes were performed to pattern multiple electrodes on few-layer $MoTe_2$ devices for four-probe measurements. The electrodes were made of 5 nm Cr/50 nm Au. Resistivity measurements were performed in PPMS with lock-in amplifiers. Speed of temperature sweep in the resistivity measurement is 5 K min^{-1}. Higher and lower sweeping speeds are performed to confirm full thermalization of the sample during the measurement. Raman measurements were performed on exfoliated few-layer $MoTe_2$ in a confocal

back-scattering geometry using a Horiba Jobin Yvon LabRAM HR Evolution spectrometer, equipped with 1800 gr mm^{-1} gratings and a liquid-nitrogen-cooled CCD. We used the $\lambda = 514$ nm line of an Argon laser for excitation. The BragGrate notch filters allow for measurements at low wave numbers. Polarized Raman spectra were measured in a-a configuration.

Acknowledgments

This project has been supported by the National Basic Research Program of China (Grant Nos. 2014CB920900, 2018YFA0305604), and the National Natural Science Foundation of China (Grant Nos. 11774010 (C Cao, X Liu and J-H Chen)) (Grant Nos. 11674013, 11704012 (D Sun)). Crystal drawings were produced by VESTA [44, 45].

ORCID iDs

Chuanwu Cao https://orcid.org/0000-0001-6778-9251
Dong Sun https://orcid.org/0000-0002-0898-4548
Shuyun Zhou https://orcid.org/0000-0002-9841-8610
Jian-Hao Chen https://orcid.org/0000-0002-9485-1759

References

[1] Radisavljevic B, Radenovic A, Brivio J, Giacometti V and Kis A 2011 Single-layer MoS_2 transistors *Nat. Nanotechnol.* **6** 147–50
[2] Wu S *et al* 2018 Observation of the quantum spin Hall effect up to 100 Kelvin in a monolayer crystal *Science* **359** 76–9
[3] Voiry D *et al* 2013 Enhanced catalytic activity in strained chemically exfoliated WS_2 nanosheets for hydrogen evolution *Nat. Mater.* **12** 850–5
[4] Zheng F *et al* 2016 On the quantum spin Hall gap of monolayer 1T'-WTe_2 *Adv. Mater.* **28** 4845–51
[5] Pan X C *et al* 2015 Pressure-driven dome-shaped superconductivity and electronic structural evolution in tungsten ditelluride *Nat. Commun.* **6** 7805
[6] Yu Y *et al* 2015 Gate-tunable phase transitions in thin flakes of 1T-TaS_2 *Nat. Nanotechnol.* **10** 270–6
[7] Liu Y *et al* 2018 Raman signatures of broken inversion symmetry and in-plane anisotropy in type-II Weyl semimetal candidate $TaIrTe_4$ *Adv. Mater.* **30** 1706402
[8] Wang Y *et al* 2017 Structural phase transition in monolayer $MoTe_2$ driven by electrostatic doping *Nature* **550** 487–91
[9] Hwang J, Zhang C and Cho K 2017 Structural and electronic phase transitions of $MoTe_2$ induced by Li ionic gating *2D Mater.* **4** 045012
[10] Kim H-J, Kang S-H, Hamada I and Son Y-W 2017 Origins of the structural phase transitions in $MoTe_2$ and WTe_2 *Phys. Rev.* B **95** 180101
[11] Ueno K and Fukushima K 2015 Changes in structure and chemical composition of α-$MoTe_2$ and β-$MoTe_2$ during heating in vacuum conditions *Appl. Phys. Express* **8** 095201
[12] Cho S *et al* 2015 Phase patterning for ohmic homojunction contact in $MoTe_2$ *Science* **349** 625–8
[13] Lai J *et al* 2018 Broadband anisotropic photoresponse of the 'Hydrogen Atom' version type-II Weyl semimetal candidate $TaIrTe_4$ *ACS Nano* **12** 4055–61
[14] Zhang K *et al* 2016 Raman signatures of inversion symmetry breaking and structural phase transition in type-II Weyl semimetal $MoTe_2$ *Nat Commun.* **7** 13552
[15] Deng K *et al* 2016 Experimental observation of topological Fermi arcs in type-II Weyl semimetal $MoTe_2$ *Nat. Phys.* **12** 1105–10
[16] Larentis S *et al* 2017 Reconfigurable complementary monolayer $MoTe_2$ field-effect transistors for integrated circuits *ACS Nano* **11** 4832–9
[17] Qian X, Liu J, Fu L and Li J 2014 Quantum spin Hall effect in two-dimensional transition metal dichalcogenides *Science* **346** 1344–7
[18] Nie S M, Song Z, Weng H and Fang Z 2015 Quantum spin Hall effect in two-dimensional transition-metal dichalcogenide haeckelites *Phys. Rev.* B **91** 235434
[19] Hughes H and Friend R 1978 Electrical resistivity anomaly in β-$MoTe_2$ (metallic behaviour) *J. Phys. C: Solid State Phys.* **11** L103
[20] He R *et al* 2018 Dimensionality-driven orthorhombic $MoTe_2$ at room temperature *Phys. Rev.* B **97** 041410
[21] Barkhausen H 1919 Zwei mit Hilfe der neuen Verstärker entdeckte Erscheinungen *Phys. Z.* **20** 401
[22] Alessandro B, Beatrice C, Bertotti G and Montorsi A 1990 Domain-wall dynamics and barkhausen effect in metallic ferromagnetic materials .1. Theory *J. Appl. Phys.* **68** 2901–7
[23] Zapperi S, Cizeau P, Durin G and Stanley H E 1998 Dynamics of a ferromagnetic domain wall: avalanches, depinning transition, and the Barkhausen effect *Phys. Rev.* B **58** 6353–66
[24] Sethna J P, Dahmen K A and Myers C R 2001 Crackling noise *Nature* **410** 242–50
[25] Spasojevic D, Bukvic S, Milosevic S and Stanley H E 1996 Barkhausen noise: elementary signals, power laws, and scaling relations *Phys. Rev.* E **54** 2531–46
[26] Das P *et al* 2010 Magnetization dynamics of a CrO_2 grain studied by micro-Hall magnetometry *Appl. Phys. Lett.* **97** 089902
[27] Chynoweth A G 1958 Barkhausen pluses in barium titanate *Phys. Rev.* **110** 1316–32
[28] Durin G and Zapperi S 2000 Scaling exponents for Barkhausen avalanches in polycrystalline and amorphous ferromagnets *Phys. Rev. Lett.* **84** 4705–8
[29] Chizhik A, Stupakiewicz A, Maziewski A, Zhukov A, Gonzalez J and Blanco J 2010 Direct observation of giant Barkhausen jumps in magnetic microwires *Appl. Phys. Lett.* **97** 012502
[30] Mai M F and Kliem H 2013 Observation of thermal Barkhausen effect in ferroelectric films of poly(vinylidene fluoride/trifluoroethylene) copolymer *J. Appl. Phys.* **114** 224104
[31] Huber-Rodriguez B *et al* 2014 Thermally driven analog of the Barkhausen effect at the metal-insulator transition in vanadium dioxide *Appl. Phys. Lett.* **105** 131902
[32] Yu G Q, Ren C, Rizwan S, Yu T, Xu K and Han X F 2013 Superconductivity-induced pinning effect in superconductor/magnetic tunnel junctions *Spin* **3** 1350006
[33] Garcia-Fornaris I, Govea-Alcaide E, Alberteris-Campos M, Mune P and Jardim R F 2010 Transport Barkhausen-like noise in uniaxially pressed $Bi_{1.65}Pb_{0.35}Sr_2Ca_2Cu_3O_{10+\delta}$ ceramic samples *Physica* C **470** 611–6
[34] Mazzetti P, Stepanescu A, Tura P, Masoero A and Puica I 2002 Barkhausen-like conductance noise in polycrystalline high-T_c superconductors immersed in a slowly varying magnetic field *Phys. Rev.* B **65** 132512
[35] Perez-Reche F J, Tadic B, Manosa L, Planes A and Vives E 2004 Driving rate effects in avalanche-mediated first-order phase transitions *Phys Rev Lett.* **93** 195701
[36] Haldar S, Vovusha H, Yadav M K, Eriksson O and Sanyal B 2015 Systematic study of structural, electronic, and optical properties of atomic-scale defects in the two-dimensional transition metal dichalcogenides MX_2 (M = Mo, W; X = S, Se, Te) *Phys. Rev.* B **92** 235408
[37] Narayan O and Fisher D S 1993 Threshold critical dynamics of driven interfaces in random media *Phys. Rev.* B **48** 7030–42

[38] Leschhorn H, Nattermann T, Stepanow S and Tang L H 1997 Driven interface depinning in a disordered medium *Ann. Phys.-Leip.* **6** 1–34
[39] Keum D H *et al* 2015 Bandgap opening in few-layered monoclinic $MoTe_2$ *Nat. Phys.* **11** 482–6
[40] Pradhan N R *et al* 2014 Field-effect transistors based on few-layered α-$MoTe_2$ *ACS Nano* **8** 5911–20
[41] Naylor C H *et al* 2016 Monolayer single-crystal 1T'-$MoTe_2$ grown by chemical vapor deposition exhibits weak antilocalization effect *Nano Lett.* **16** 4297–304
[42] Yamamoto M *et al* 2014 Strong enhancement of Raman scattering from a bulk-inactive vibrational mode in few-layer $MoTe_2$ *ACS Nano* **8** 3895–903
[43] Qi Y *et al* 2016 Superconductivity in Weyl semimetal candidate $MoTe_2$ *Nat. Commun.* **7** 11038
[44] Momma K and Izumi F 2011 VEST A 3 for three-dimensional visualization of crystal, volumetric and morphology data *J. Appl. Crystallogr.* **44** 1272–6
[45] Brown B E 1966 The crystal structures of WTe2 and high-temperature $MoTe_2$ *Acta Crystallogr.* **20** 268–74